# Advective pore-water exchange driven by surface gravity waves and its ecological implications

*Elimar Precht*[1] *and Markus Huettel*
Max Planck Institute for Marine Microbiology, Celsiusstrasse 1, D-28359 Bremen, Germany

### Abstract

The effects of surface gravity waves on pore-water release from permeable sediment ($k = 1.3$–$1.8 \times 10^{-11}$ m²) in shallow water were studied in a wave tank. Our tracer experiments demonstrated that shallow-water waves can increase fluid exchange between sandy sediment and overlying water 50-fold, relative to the exchange by molecular diffusion. The main driving force for this increased exchange are the pressure gradients generated by the interaction of oscillating boundary flows and sediment wave ripples. These gradients produce a pore-water flow field, with a regular pattern of intrusion and release zones, that migrates with ripple propagation. The ensuing topography-related filtering rates in the wave tank ranged from 60 to 590 L m$^{-2}$ d$^{-1}$ and exceeded the solute exchange rates caused by hydrostatic wave pumping (38 L m$^{-2}$ d$^{-1}$) and initial molecular diffusion (corresponding to 10–12 L m$^{-2}$ d$^{-1}$). Wave-induced filtration is ecologically relevant because permeable sandy sediments are very abundant on the continental margins and can be converted into effective filter systems, which suggests that these sediments are sites for rapid mineralization and recycling. We propose that the wave influenced continental shelf may be subdivided into two zones: a shallow zone (water depth < wavelength/2), where wave orbital motion at the sea floor creates ripples and causes topography related advective filtering; and a deeper zone (wavelength/2 < water depth < wavelength), where wave pumping enhances interfacial exchange by hydrostatic pressure oscillations.

Physical and biological transport link the biogeochemical processes in the water column and sediment. Whereas molecular diffusion and, locally, also bioturbation are the major transport mechanisms in the cohesive, fine-grained deep-sea deposits (Berner 1980; Aller 1982, 2001), solute transport caused by pore-water flows increases in importance in permeable sandy shelf sediments. Here, boundary layer flows, interacting with sea-bed topography, induce pressure differences at the sediment-water interface that lead to pore-water motion in permeable sediments. The ensuing advective transport can exceed transport by molecular diffusion by several orders of magnitude (Huettel and Webster 2001).

In areas where water depth ($D$) is smaller than half the wavelength ($\lambda$) of the surface gravity waves, oscillating flows are generated at the sediment-water interface by the wave orbital-water motion (e.g., Denny 1988). Webb and Theodor (1968, 1972) showed, by injecting dyed water into coarse sandy nearshore sediment and observing its reappearance at the sediment surface, that such oscillating boundary flows could drive sediment-water–interfacial fluxes. The trajectories of pore-water particles under a rippled bed over one wave period were calculated by Shum (1992). His results suggested that the zone of advection extends several ripple heights below the sediment surface over a wide range of wave conditions and sediment characteristics. Indications that surface gravity waves may be relevant for the cycling of matter in shallow environments were reported by Oldham and Lavery (1999), who measured an increased release of nutrient-rich pore water from estuarine sediment and attributed this enhancement to the effect of waves.

For pore-water exchange driven by wave-related hydrostatic pressure oscillations, Riedl et al. (1972) introduced the term "subtidal pump." On the basis of field observations, those authors presented model calculations that suggested that the subtidal pump could filter the complete ocean volume in only 14,000 yr. Rutgers van der Loeff (1981) described the same process as increased diffusivity in the upper 1–1.5 cm of intertidal sandy sediment under low to moderate wave action. To include the wave pumping in their in situ flux measurements, Malan and McLachlan (1991) deployed benthic chambers with flexible membrane tops that revealed that oxygen consumption and solute fluxes are positively correlated with wave action. However, it is not obvious how the circular motion of pore water within sediment can cause net solute transport, because the displacement through the wave cycle guides the fluid back to its origin. To explain net transport, Harrison et al. (1983) included mechanical dispersion in the subtidal pump theory. In contrast to shear dispersion, the rotational dispersion caused by waves does not rely on molecular diffusion to be effective but requires that the direction of the pressure gradient rotate with time (Webster et al. 1996). The results of rotational dispersion are similar to those of diffusive processes; however, it can be many times more effective than molecular diffusion or shear dispersion as a transport mechanism.

These transport studies suggest that waves, by enhancing fluid exchange between sediment and overlying water, also affect the biogeochemical processes in permeable beds. Modeled oxygen distributions underneath a rippled surface exposed to progressing waves have suggested that, in permeable beds, concentration gradients in the horizontal can be in the same order of magnitude as those in the vertical
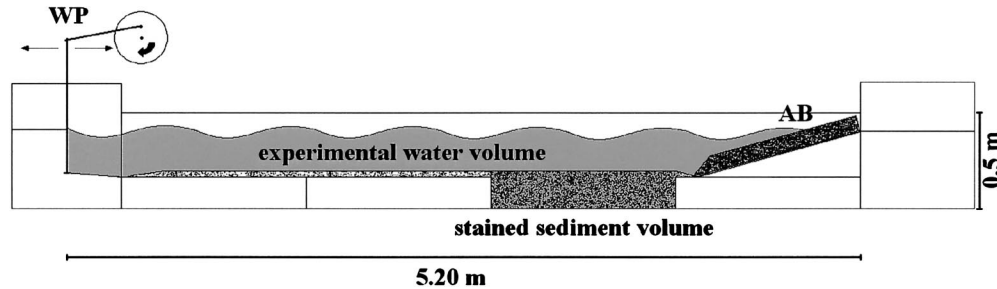
Fig. 1.   The laboratory wave tank (light gray, sealed off water volume; dark gray, experimental water volume; WP, wave paddle; AB, artificial beach).

(Shum 1993). These findings demonstrate that the classical one-dimensional approach frequently used to describe the distribution of pore-water constituents and to assess the related fluxes across the sediment-water interface is inadequate for sandy, permeable sea beds (Shum and Sundby 1996).

The potential relevance of wave-induced advective pore-water exchange for metabolic processes in permeable shelf sands may be inferred from results obtained in flume studies that have addressed advective pore-water exchange driven by unidirectional flows. Those studies showed that advective interfacial fluid transport provides a rapid pathway for suspended organic particles and phytoplankton cells into permeable sediments (Huettel et al. 1996; Huettel and Rusch 2000). Simultaneously, oxygen can be transported advectively deep into the bed (Shum 1993; Ziebis et al. 1996), which enhances the mineralization of this material (Forster et al. 1996). The advectively induced pore-water flow field in sediment generates a complex biogeochemical zonation with areas of enhanced nitrification or iron precipitation and vertical channels through which ammonium and reduced metals are transported to the sediment surface (Huettel et al. 1998).

The aim of the present study was to characterize and quantify the effects of surface gravity waves on fluid exchange between a sandy bed and the overlying water column and to investigate the mechanisms leading to wave-induced interfacial exchanges. To achieve this, a set of laboratory wave-tank experiments was conducted with sandy sediment stained with the conservative soluble tracer Rhodamine WT. The use of Rhodamine WT allowed the synchronous quantification of the interfacial flux and visualization of the evolving pore-water flow pattern.

## Materials and methods

*Wave-tank setup*—Four experiments (experiments [Exp] 1–4) were carried out in a laboratory wave tank. The wave tank was made of clear acrylic and had an open channel section of 520 cm length with rectangular cross-section (50 cm high $\times$ 47 cm wide). Two acrylic boxes ("upstream" box, 240 cm long and "downstream" box, 120 cm long; both 19 cm high and spanning the width of the channel) were placed into the open channel section, such that the opening between the two boxes enclosed a section of 120 cm length that could be filled with sediment (Fig. 1). Waves were generated at the upstream end of the wave tank with a

paddle driven by an electric motor. The wave amplitude was controlled by the stroke of the eccentric, and the wave frequency could be adjusted via the motor speed. This setup permitted the reproducible generation of sinusoidal waves of selected amplitude and frequency. At the downstream end of the wave tank, the dissipation of the waves was achieved by an artificial beach made of an acrylic wedge of 1 m length that caused the waves to run up and break. In Exps 3 and 4, this wedge was additionally covered by a 10-cm-thick mat of highly permeable plastic foam, to maximize the dissipation of the wave energy. The open channel section was sealed from the other parts of the wave tank and from the two inset acrylic boxes, to prevent loss of the tracer into those sections.

All experiments were conducted with propagating waves. Amplitudes, wavelengths, and frequencies are listed in Table 1. The hydrodynamic conditions in Exps 3 and 4 were identical.

*Sediment preparation and sampling*—The experimental sediment was cleaned, and sieved, dry quartz sand originating from the Weser river estuary (in northern Germany) with a grain size distribution of 100–300 $\mu$m and was mixed with Rhodamine WT tracer solution, which gave it a pink appearance. The initial tracer concentrations for the respective experiments are listed in Table 1. The saturated pink sediment was inserted into the trough enclosed by the two acrylic boxes, to produce a sediment layer of 25 (Exp 1) or 22 (Exps 2–4) cm depth with 141 and 124 dm$^3$ volume, respectively. The two boxes in the open channel section were covered with 6 (Exp 1) or 3 (Exps 2–4) cm of unstained sand of identical grain size. The sediment was compacted by the application of low-frequency vibration, and the surface was carefully smoothed before each experiment, to create an overall even surface with uniform roughness in the open channel section. Ripple evolution occurred as a response of the bed to the applied wave action.

The use of Rhodamine WT as a tracer to stain the sediments had two functions. First, sequential water sampling during the experiments and subsequent analysis of the tracer content of the samples allowed the assessment of the flux of pore water from the sediment over time. Second, the red color of Rhodamine WT allowed direct observation of the evolving pore-water flow patterns in the sediment.

Directly before and after each wave-tank experiment, sediment subcores of 2.6 cm diameter and 10 cm length were

Table 1. Summary of experimental parameters. Permeabilities, porosities, and tracer concentrations are initial values. Variability in initial permeability and porosity values are due to different degrees of compaction of the sediment.

| Experiment | Exp 1 | Exp 2 | Exp 3 | Exp 4 | Diff 1 | Diff 2 |
|---|---|---|---|---|---|---|
| Start | 14 Sep 1999 | 16 Sep 1999 | 11 Jul 2000 | 14 Nov 2000 | 22 Jun 1999 | 11 Jul 2000 |
| End | 15 Sep 1999 | 17 Sep 1999 | 12 Jul 2000 | 15 Nov 2000 | 24 Jun 1999 | 12 Jul 2000 |
| Duration (h) | 14.75 | 19.4 | 24 | 24 | 72 | 24 |
| Sediment* | | | | | | |
|   Permeability ($m^2$) | $1.32\times10^{-11}$ | $1.32\times10^{-11}$ | $1.79\times10^{-11}$ | $1.82\times10^{-11}$ | $2.02\times10^{-11}$ | $1.75\times10^{-11}$ |
|   Porosity (vol%) | 36.6 | 36.9 | 37.3 | 38.1 | 38.25 | 37.7 |
|   Sediment depth (cm) | 22 | 21.5 | 22 | 22 | 22 | 20.5 |
|   Water | | | Fresh, 19°C | | | |
| Tracer | | | Rhodamine WT | | Brilliant Blue | Rhodamine WT |
|   Tracer concentration ($\mu$mol $L^{-1}$) | 40 | 39 | 21 | 5 | 47 | 19 |
|   Water depth (cm) | 15 | 20 | 17 | 17 | 17 | 17 |
| Wave | | Propagating | | | None | |
|   Amplitude (cm) | 8 | 9 | 6 | 6 | — | — |
|   Length (cm) | 60 | 80 | 60 | 60 | — | — |
|   Frequency (Hz) | 1.56 | 1.2 | 1.3 | 1.3 | — | — |

\* Quartz sand, 100–300 $\mu$m.

taken from the experimental sediment volume for porosity, permeability, and tracer distribution analyses. Additionally, several surface sediment samples (1 cm in diameter × 2.5 cm long) were taken after Exps 3 and 4 using cutoff syringes. After carefully replacing the retrieved sediment volumes with equally stained sediment, the wave tank was filled with ~1,750 liters of freshwater. The water level in the channel was raised very slowly, to minimize tracer release from the sediment. The water volume in the channel that could exchange with the sediment pore water amounted to 360 liters in Exps 1 and 2 and 410 liters in Exps 3 and 4. Table 1 gives an overview of the experimental parameters.

*Diffusion experiments*—Two sets of diffusion experiments (diffusion [Diff] 1 and 2) were set up in three acrylic cylindrical chambers (19 cm inner diameter × 40 cm high) with stained sediment, to assess the diffusive release of tracer from the sediment. The experimental parameters are presented in Table 1. After compaction, sediment subcores were taken from each chamber and prepared for analysis of tracer content, permeability, and porosity, as described above for the subcores from the wave tank. After the extracted sediment volumes had been replaced by stained sediment, the sediment surfaces were covered with a plastic film, and 4.25 liters of freshwater were added to each chamber without mixing with the stained pore water. Then the plastic films were removed, and the chambers were kept under stagnant conditions for the duration of the experiments. At regular time intervals, the water column of each chamber was gently mixed by five horizontal strokes with a spatula to homogenize tracer distribution, and water samples (3 × 2 $cm^3$) were taken and stored for later analysis of their Rhodamine WT content. After the experiments, the chambers were carefully drained, and a second set of sediment subcores was taken for analyses of tracer gradient over depth, permeability, and porosity.

*Analyses*—The sediment subcores taken from the laboratory wave tank, and the diffusion chambers were sectioned into 1-cm-thick horizontal slices for pore-water and porosity analysis. The porosity of the sediment samples of the respective cores was calculated from the wet and dry (after 48 h drying at 60°C) weights of the sediment slices.

Pore-water extraction was achieved by centrifugation at 2,900 × g for 10 min at 10°C. The extracted pore water was analyzed for its Rhodamine content by spectrophotometry (absorption, 556 nm) or fluorescence spectrophotometry (excitation, 570 nm and emission, 556 nm). The absolute tracer concentrations of the analyzed samples were calculated from the extinction coefficient for Rhodamine WT.

The sediment subcores used to assess the permeability were sealed after sampling and stored at 4°C until the measurements were carried out, usually within a few days. Permeability was assessed using a constant head permeameter (Klute and Dirksen 1986), and values for the dynamic viscosity ($\eta$) were calculated according to the method of Krögel (1997).

During all experiments, water samples were collected at preset time intervals, with the shortest intervals during the initial phase of the experiments. After starting the wave experiments, a tracer cloud developed over the stained sediment that then dispersed over the entire volume of the open channel section. Our flux calculations, therefore, are based on the integrated dye content of the entire channel. Samples (3 × 5 ml) were taken at six representative positions from the experimental water volume and also from the sealed off sections of the wave tank, to assess tracer loss due to possible leakages into the sealed sections. The water samples were stored at 10°C and subsequently analyzed for their tracer content, to determine the flux of tracer between sediment and water.

Hydrodynamics were measured using a three-beam DAN-TEC laser Doppler anemometer (LDA) system in the back-

Table 2. Summary of the experimental results.

| Experiment | Exp 1 | Exp 2 | Exp 3 | Exp 4 | Diff 1 | Diff 2 |
|---|---|---|---|---|---|---|
| Ripple length (cm) | 3 | 3 | 2.5 | 2.5 | — | — |
| Ripple height (cm) | 0.7 | 0.7 | 0.5 | 0.5 | — | — |
| Ripple height/length ratio | 0.23 | 0.23 | 0.2 | 0.2 | — | — |
| First ripples evolved (min) | 15 | 5 | 10 | 20 | — | — |
| Initial ripple evolution | Complete | Complete | Half of the sediment surface | Patchy | — | — |
| Calculated washout depth (cm)/after (h) | 2.6/14 | 3.0/17 | 3.1/24 | 3.2/24 | 0.8/24 | 0.7/24 |
| Calculated washout depth after 2 h (cm) | 2.6 | 2.2 | 0.9 | 1 | 0.2 | 0.3 |
| Tracer exchange rate (L m$^{-2}$ d$^{-1}$) | 222 | 590 | 60 | 93 | 12 (1st h) | 10 (1st h) |

scatter mode during all experiments except Exp 4. This LDA technique allows three-dimensional measurements of the flow velocity in a spheroidal measuring volume as small as 70 $\mu$m in diameter. During Exp 3, two vertical profiles (100–2 mm above the sediment) of the horizontal ($u$) and vertical ($v$) velocities were measured 150 min after the start of the experiment above an unrippled section of the experimental sediment surface. In the water layer closer than 6 mm to the sediment-water interface, the LDA setup only allowed the measurement of the $u$ velocity component.

## Results

*Pore-water flow pattern*—The waves caused advective pore-water exchange in the wave tank that exceeded the maximum diffusive exchange (based on exchange rate in the first hour) in the stagnant control tank by factor 8–54. This flux enhancement was mainly caused by pore-water flows driven by oscillating boundary flows interacting with the wave-generated sediment ripples. The small flux enhancements prior to the development of the ripple topography revealed that the sinusoidal hydrostatic pressure oscillations due to the passage of the surface gravity waves ("wave pumping") had relatively little influence on the pore-water exchange. Table 2 summarizes the results of the wave-tank and diffusion experiments.

In the wave-tank experiments, four phases could be distinguished after the initiation of the waves:

1. The initial phase was characterized by a smooth sediment surface and moderate tracer release from the sediment. During this phase, diffusion, wave pumping (sensu Riedl et al. 1972), and some advective release linked to small-scale topography elements remaining on the smoothed sediment surface drove the interfacial solute flux.
2. The transitional phase started with the onset of ripple formation and ended when the entire sediment surface was covered with ripples. Within this period, the contribution of advective interfacial tracer exchange caused by ripple-flow interaction increased rapidly. At the end of this phase, solute release rates reached their maxima.

3. The flushing phase occurred when the tracer was advectively washed from the upper sediment layer mainly because of oscillating flow–ripple interaction. Because of rapid tracer removal, its release rates decreased during this phase.
4. The final equilibrium phase occurred when the tracer release was limited by the diffusion of tracer from deeper sediment layers into the flushed layer, with the concentration gradient not situated at the sediment-water interface but at the lower limit of the washout zones.

Figure 2a–c shows the initial (Fig. 2a) tracer distribution in the sediment and the distribution after 20 min (Fig. 2b) and 24 h (Fig. 2c) during Exp 3. Ripple formation started 10 min into the experiment.

During the initial phase, wave action removed the red dye from the upper 1–2 mm of the sediment, producing a thin, uniform washout layer. During ripple formation, light-colored washout zones free of tracer formed rapidly in the ripple troughs, where water was forced into the sediment. This fluid intrusion was balanced by the release of pore water from confined upwelling zones at the ripple crests (Fig. 2b,d,e). This pore-water flow pattern was firmly linked to the sediment ripples (Fig. 2d,f) and propagated with ripple migration. Later during the experiment, sediment bars (Rey et al. 1995) formed with wavelengths of ~30 cm and amplitudes of ~1 cm. Such bars are formed by resonance effects that exist in wave tanks because of partial wave reflection. Ripples were larger on the bar crests and smaller in the bar troughs. Intrusion and release zones linked to ripple and bar topographies combined to form larger irregular areas of down- and upwelling (Fig. 2c).

Figure 2f shows an area of sediment surface that displayed no ripples until 23 h after the start of Exp 3. This section permitted the direct comparison of tracer washout caused by hydrostatic wave pumping and topography-flow interaction. Whereas areas with ripples were characterized by washout zones and pore-water upwelling zones reaching the sediment surface, this smooth area displayed only a very thin uninterrupted surface layer depleted in tracer comparable to that observed during the initial phase of the experiment. This
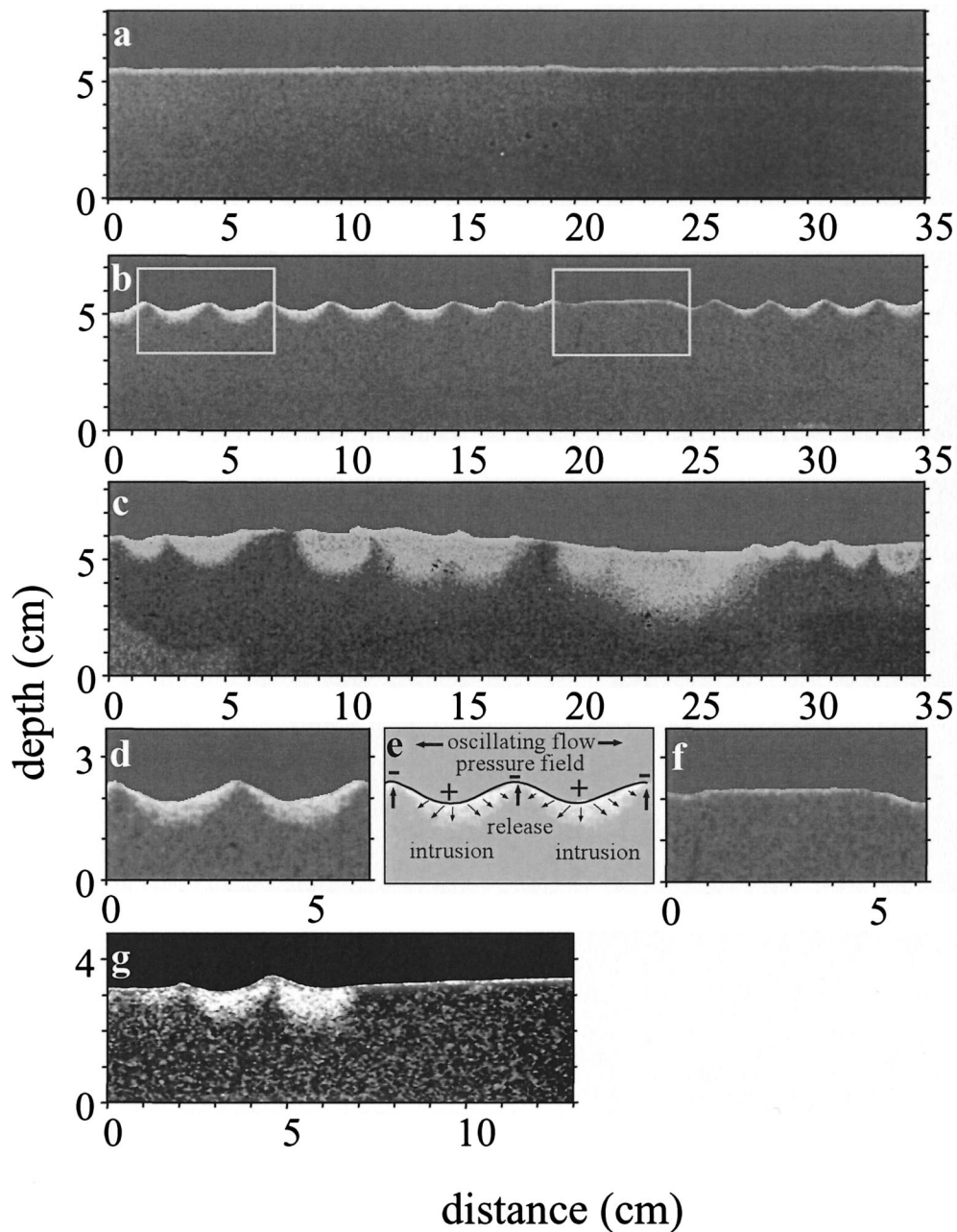
Fig. 2. Evolution of the washout pattern during Exp 3. Dark areas of the sediment indicate a high Rhodamine content; red and contrast were digitally enhanced before the figure was changed to grayscale. (a) Before the experiment, when there was a smooth sediment surface; (b) after 20 min (boxes indicate the sectors magnified in panels d and f); (c) after 24 h; (d) magnified from panel b, after 20 min; (e) sketch of the pore-water flow pattern and the current-induced pressure field; (f) magnified from panel b, after 20 min; (g) exceptional area, where ripples had not formed by 23 h.

contrast reveals the dominance of the topography-related pore-water release.

Because ripple formation did not take place in the same manner in all experiments, the release of tracer varied as well. In Exps 1 and 2, ripples covered the complete experimental sediment surface after 45 min. This resulted in a pronounced peak of tracer release. In Exp 2, tracer release increased sharply after 50 min and started to level out after 105 min (Fig. 3). The first derivative of tracer concentration over time yielded the filtration rate (Fig. 3), which in Exp 2 peaked at 590 L m$^{-2}$ d$^{-1}$. During the other experiments, the filtration rates ranged from 222 (Exp 1) to 60 and 93 (Exps 3 and 4, respectively) L m$^{-2}$ d$^{-1}$. In comparison, the tracer volume released by diffusion from the sediments under stag-
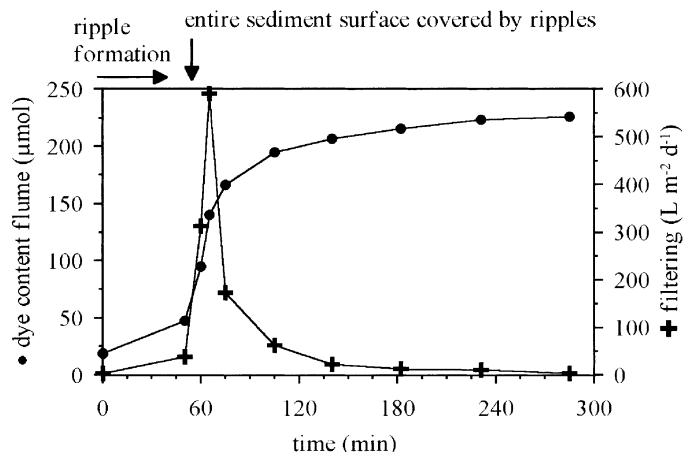
Fig. 3.   Tracer release (solid circles) and derived filtering rates (crosses) during Exp 2.

nant water columns during the first hour of the experiments corresponded to a fluid exchange of ~12 and 10 L m$^{-2}$ d$^{-1}$ for Diffs 1 and 2. All experiments are summarized in Fig. 4, which gives a picture of the sediment depths that theoretically had to be completely flushed of tracer to explain its concentration increase in the water column over time during the different experiments. This normalized tracer release for water volume, sediment surface area, and porosity, such that all experiments became directly comparable. Figure 4 demonstrates that the four wave-tank experiments showed a much stronger initial tracer release pulse from the sediment than the diffusion experiments under stagnant conditions. In all experiments, the high initial fluxes leveled out after a few hours and approached values on the order of the diffusive release because most of the tracer was then flushed from the upper sediment layer. Consequently, total tracer release rates at the end of all flume runs were similar. After 24 h, the total release of tracer from the sediment under waves still
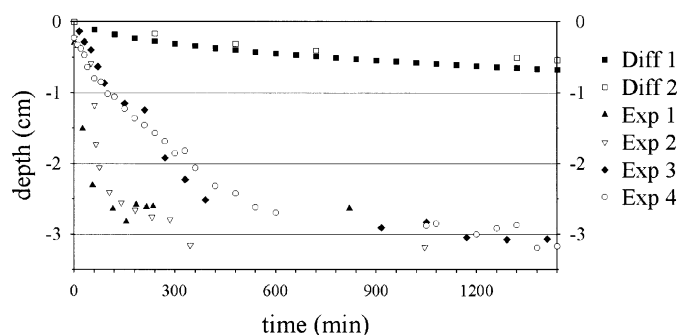


Fig. 4.   Dye release during the wave experiments (Exps 1–4) and the control diffusion chambers (Diff 1, Brilliant Blue; Diff 2, Rhodamine WT) into the water, expressed as theoretical sediment depths completely flushed free of dye—this form of presentation is independent of initial tracer concentrations, sediment surface area, and experimental water volume. In reality, washout affected larger depths than this theoretical depth. The calculation assumed complete washout; however, observed horizontal dye concentration gradients in the sediment demonstrated that washout depths varied locally.
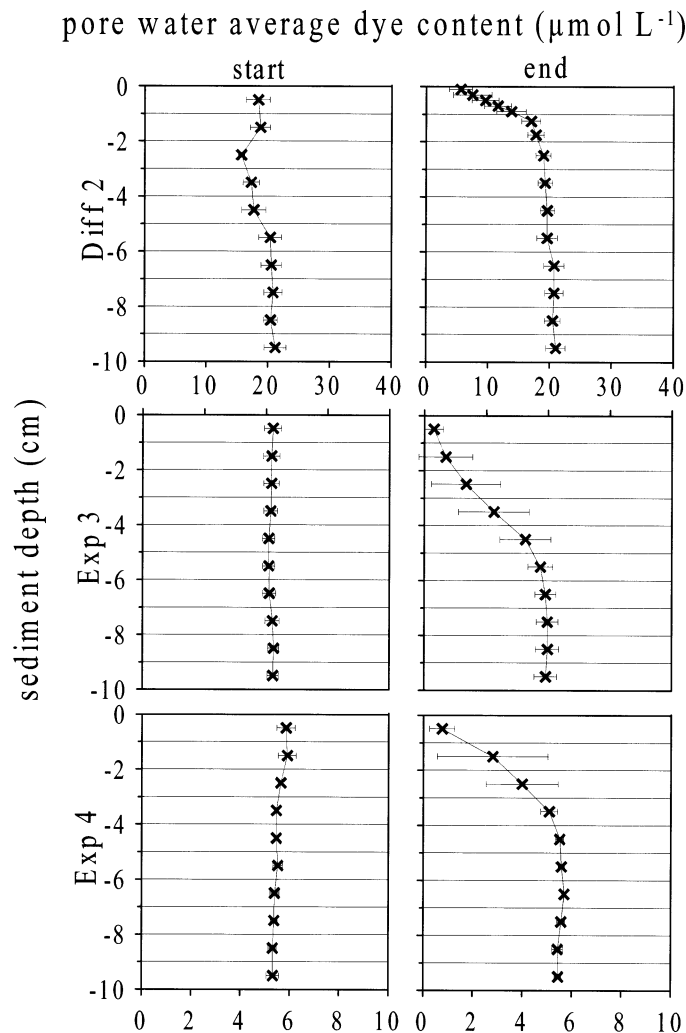


Fig. 5.   Average sediment pore-water dye concentration distributions over depth before and after Exps 3 and 4 (same wave settings) and Diff 2: (left) before the experiment and (right) after the experiment. Error bars show the standard deviation.

was four to six times higher than that under stagnant conditions, and the final theoretical depth of complete flushing during all wave experiments was ~3 cm.

The analyses of the pore water from the sediment cores taken before and after the experiments quantified the vertical concentration gradients that had developed in the sediment. These gradients confirmed the theoretical washout depths inferred from the water samples, because both methods yielded the same results. The initial tracer distributions showed homogeneous concentrations over all depths with little scatter (Fig. 5). The cores taken after Exps 3 and 4 revealed that the averaged release of tracer affected the sediment down to ~4 cm depth. This was four times higher than in the diffusive cores, where reduced tracer concentrations were detectable only down to 1 cm. The error bars reflect the horizontal variations of tracer concentration that characterized the washout zone between 1 and 3 cm sediment depth.

*Hydrodynamics*—The wavelengths ($\lambda$) of the propagating waves ranged from 60 to 80 cm and the water depths ($d$)
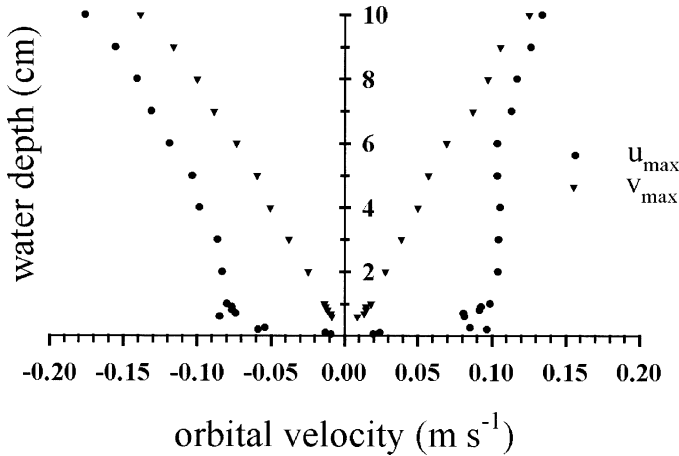
Fig. 6. Profiles of maximum orbital velocities measured with the LDA at the beginning of Exp 3 above unrippled experimental sediment surface; solid circles indicate maximum horizontal velocity ($u$) and solid triangles indicate maximum vertical velocities ($v$). Values of $v$ decreased linearly and values of $u$ decreased nonlinearly. Between 0 and 0.6 cm above the sediment surface, the LDA setup only allowed for the measurement of $u$.

from 15 to 20 cm. With $d < \lambda/2$, oscillating water motion was present at the sediment-water interface.

Figure 6 shows the mean maximal orbital velocities $u_{max}$ and $v_{max}$ for each depth, measured over the smooth sediment surface at the beginning of Exp 3. The maximum boundary shear stress can be calculated using the velocity gradient in the viscous sublayer:

$$\tau_{0m} = \rho\nu(\delta u/\delta z) \tag{1}$$

with density $\rho$, dynamic viscosity $\nu$, velocity in $x$-direction $u$, and height over sediment $z$ (Caldwell and Chriss 1979). With an averaged maximum value of 0.1 m s$^{-1}$ for $\delta u$ for a $\delta z$ of 0.1 cm, directly over the sediment surface, this results in $\tau_{0m} = 0.107$ N m$^{-2}$. Inferred from

$$u_{*max} = (\tau_{0m}/\rho)^{1/2} \tag{2}$$

the maximum shear velocity $u_{*max} = 0.01$ m s$^{-1}$. Assessing $u_{*max}$ from a log velocity profile yields a similar result, with $u_{*max} = 0.012$ m s$^{-1}$, which results in $\tau_{0m} = 0.148$ N m$^{-2}$.

*Ripple formation*—The shear velocity required to move a sediment particle of our sediment (calculated according to $u_* = 0.06\sqrt{(\rho_s - \rho_f)gD}$, where $\rho_s$ is the density of the sand grains, $\rho_f$ is the density of the fluid, $g$ is gravitational acceleration, and $D$ is the grain diameter; Hsü 1989) was smaller and ranged 0.0024–0.0042 m s$^{-1}$. Consequently, ripples started forming on parts of the sediment surface within the initial 20 min of all wave experiments (Table 2). Even though the sediment surface was carefully leveled and smoothed before the experiments started, a few small roughness elements of up to 1 mm height were still existent, and ripple formation started at these areas. From the zones of initial ripple formation, the ripples spread over the entire experimental sediment area, which took 60 and 15 min in Exps 1 and 2, respectively, and 8–10 h in Exps 3 and 4. The ripples migrated in the same direction as the waves propa-

gated, and their initial migration speed ranged between 2 and 3 cm h$^{-1}$.

## Discussion

*Advection and wave pumping*—Our experiments show that wave-induced oscillating flows interacting with sediment topography drive advective processes in a manner similar to that of unidirectional flow, as described by, for example, Savant et al. (1987), Thibodeaux and Boyle (1987), or Huettel and Gust (1992). Under oscillating flow, water is forced into the sediment at the ripple troughs and flanks, and pore water emerges centered at the ripple crest, as predicted by Shum's (1992) model calculations. According to Rutherford et al. (1995), the pressure perturbation along a sediment dune (ripple) surface is sinusoid, with a wavelength equal to the dune wavelength. This could be confirmed in our experiments for the flow fields that developed under oscillating flows, because washout was closely linked to ripple (and bar) wavelength. Likewise, applying mathematical models developed for the estimation of filtration rates caused by unidirectional flows to our settings produced exchange rates that were close to those we measured in the wave experiments. If we assumed that oscillating flows produce pressure gradients at protruding topography in a manner similar to unidirectional flows, the pressure perturbation at each ripple was estimated by

$$p = 0.14\rho u^2(\delta/0.34d)^{3/8} \tag{3}$$

for $\delta/H \leq 0.34$ with ripple height $\delta$, water depth $d$, density $\rho$, and mean current velocity $u$ (Elliott 1990; Huettel and Webster 2001). For $u$ we used a root-mean square value of the oscillating horizontal velocity component that was 0.112 m s$^{-1}$ at 10-cm water depth in Exp 3. From this pressure perturbation, the fluid exchange rate $w_0$ could be calculated according to

$$w_0 = (2k/\rho\nu L_D)p \tag{4}$$

with $k$, $\nu$, and $L_D$ denoting permeability, kinematic viscosity, and decay length (the length scale of the ripple), respectively (Huettel and Webster 2001). Using the parameters and ripple dimensions of Exp 3, this gives a mean pressure perturbation of 1.11 Pa, which yields a theoretical flushing rate of 116 L m$^{-2}$ d$^{-1}$. The bars of 30-cm amplitude and 1-cm height would additionally contribute 12 L m$^{-2}$ d$^{-1}$ of filtration. The resulting total flushing rate of 128 L m$^{-2}$ d$^{-1}$ is in the same order of magnitude as the ones measured in our experiments.

It is clear that the wave-generated flow–topography interaction addressed in the present study only can cause filtration where the orbital motion reaches the sea bed (depth < wavelength/2). However, surface gravity waves cause filtration beyond that depth as well, because of the hydrostatic pressure oscillations they produce.

Riedl et al. (1972) estimated that, averaged over the global continental margin, wave pumping filters ~33 L m$^{-2}$ d$^{-1}$ through sandy shelf sediments. Mu et al. (1999) calculated a seepage of 15 L m$^{-2}$ d$^{-1}$ into and out of a flat sandy (*md* = 164 $\mu$m) seabed at 15 m water depth caused by wave-induced hydrostatic pressure oscillations (wave height = 1.5 m; length = 10 m, period = 6 s), which suggests a sub-

stantially smaller filtration rate than that proposed by Riedl et al. (1972).

Our experimental setup was not designed to quantify wave pumping. Nevertheless, the initial phase of Exp 2, when a rippled surface topography had not yet developed, may have indicated the magnitude of the effect of hydrostatic pressure oscillations on pore-water release (Fig. 2). During this phase, we recorded a filtration rate of 38 L m$^{-2}$ d$^{-1}$. This rate must be treated as a maximum estimate, because, in our flume experiments, the ratio between sediment permeability and water depth was large relative to most areas in the shelf. However, because this rate is in the range of the findings of Mu et al. (1999) and Riedl et al. (1972), we used this value as an approximation for the effects of wave pumping. The comparison of this rate and the filtration rate caused by oscillating flow–topography interaction suggests that, where wave orbital motion reaches the seabed, oscillating flow–topography interaction is more effective for pore-water exchange than wave pumping.

In our wave tank, exchange rates caused by oscillating flow–topography interaction reached up to 590 L m$^{-2}$ d$^{-1}$. Because our calculations were based on the maximum observable pulse of tracer release from the sediment, the resulting estimates of the water volume filtered through the sediment by wave action are minimum values. This is because the pulse maximum depends on how fast the ripples are formed, as shown by the delayed release of tracer during Exps 3 and 4, during which ripples initially formed on half the sediment surface (Exp 3) or were patchy over the duration of several hours (Exp 4). It is likely that, in these two experiments, the final filtration rates with fully developed sediment topography were higher, but by that time an assessment of the effective filtration was impossible because most of the tracer had already been washed from the upper sediment layers.

Oscillating flow–topography interaction caused a clear increase of the interfacial tracer flux relative to the controls with stagnant water, but how applicable are these results to natural environments? In shallow littoral regions, hydrodynamic settings almost identical to our flume settings may be found, and in such environments we can expect effects on pore-water exchange similar to those we observed in the laboratory. In situ measurements by Precht and Huettel (unpubl. data) in a littoral zone (70 cm water depth) with sands of comparable permeability revealed filtration rates very similar to those recorded in the wave tank. The visual observations of dye transport by Webb and Theodor (1968) confirm this transport process for a permeable rippled bed at 3 m depth. Similar observations could be made in a rippled carbonate sand bed at 18 m water depth off the East coast of Oahu (M.H. unpubl. data). Wave ripples on the seabed are frequently found in areas with water depths <100 m (e.g., Cacchione et al. 1999; Ogston and Sternberg 1999). These ripples disclose that surface gravity waves generated substantial oscillating flows at these depths that were capable of moving sediment. Where the sediment is permeable enough, such flows will generate advective pore-water exchange.

*Natural environments*—Large sections of the world's shelf areas display conditions that allow advective processes to occur: they are covered by permeable sandy sediments, display sediment topography in form of ripples, and are permanently or episodically reached by oscillating currents. Waves dominate sediment dynamics in large shelf areas, with the majority of sediment-transport occurring during times of energetic long period waves (e.g., Wiberg and Harris 1994; Harris and Wiberg 1997). The extension of the shelf areas affected by waves was numerically assessed by Harris and Coleman (1998) with the result that, for example, in the North Atlantic, wave climate was such that quartz sands of 100 $\mu$m diameter would be mobilized down to a
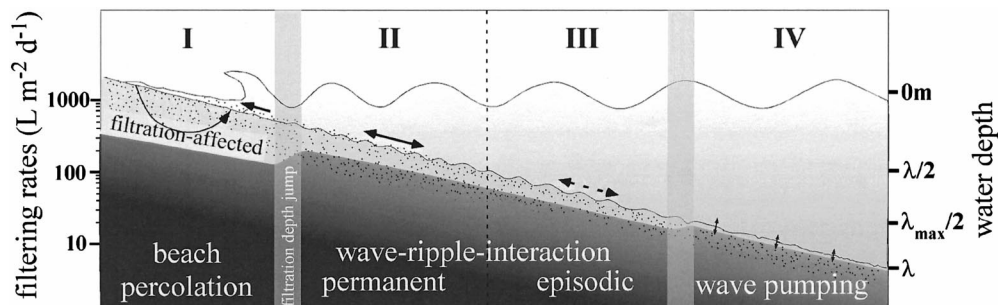


Fig. 7. Schematic overview of the different sediment-water interaction processes due to surface gravity waves in coastal and shelf environments ($\lambda$ = wavelength). (I) In the beach zone, beach percolation can lead to very high filtering rates in a zone of limited lateral extension. In lower parts of the beach, resuspension and high sediment mobility can lead to pore-water release and particulate organic matter burial. (II) In the permanent advection zone (water depth $< \lambda/2$), surface gravity waves permanently induce oscillating boundary flow that, by interacting with sediment ripples, lead to constant advective solute exchange. This advective flushing of the upper sediment layers leads to a relatively thick oxygenated sediment layer and particle transport into the bed. (III) In the episodic advection zone (water depth $< \lambda_{max}/2$), episodic advection is due to oscillating flow-sediment topography interaction (*see Fig. 8*). (IV) In the wave pumping zone ($\lambda/2 <$ water depth $< \lambda$), waves are only effective for the interfacial exchange due to pumping caused by hydrostatic pressure oscillations. In deeper areas, interfacial transport is governed by diffusion and bioirrigation.
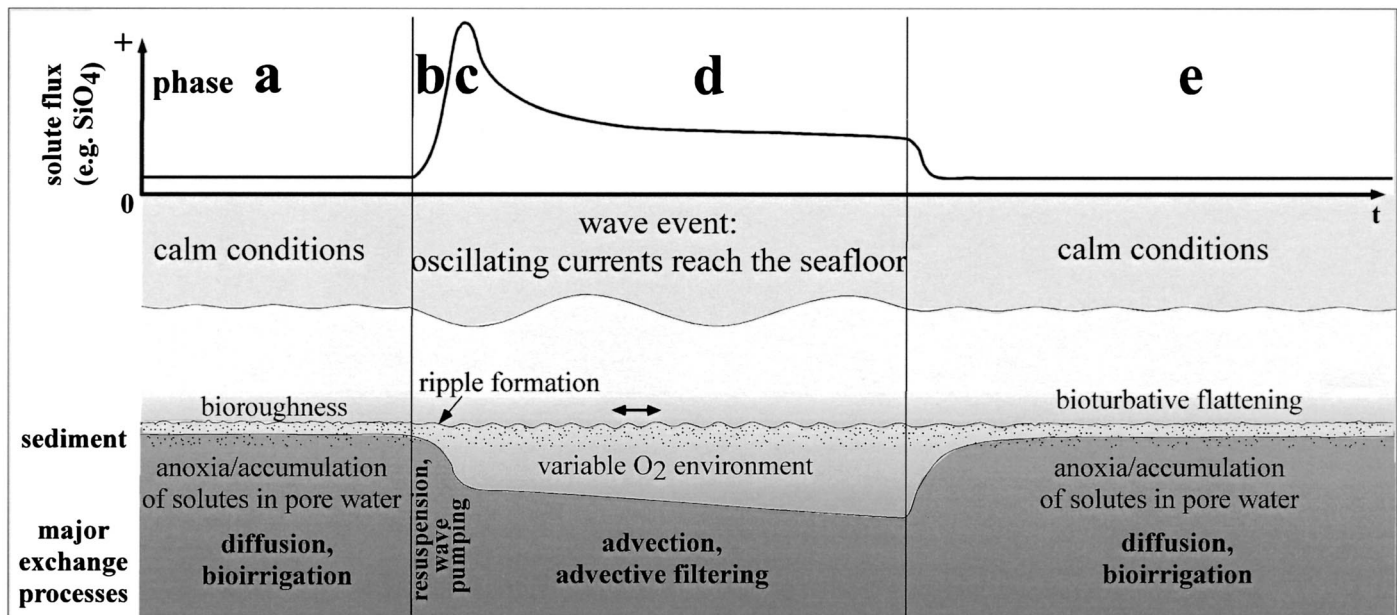
Fig. 8.    Schematic overview of sediment water–interface processes in areas episodically affected by wave events. (a, calm phase) In the absence of effective interfacial transport mechanisms, permeable sandy sediments may accumulate solutes (e.g., silicate) and small particles in their pore space. (b, wave phase) At the beginning of a wave event, the exchange between the permeable sediment and the overlying water may be driven by advection linked to oscillating flow interacting with sediment topography (e.g., bioroughness; Huettel and Gust 1992; Oldham and Lavery 1999) or existing relict ripples. (c, wave phase) With continuing wave action, oscillating bottom currents generate sediment ripples. Boundary flow–ripple interaction causes advective filtering that exchanges the pore water of the upper sediment layer; therefore, a maximum advective solute release takes place. (d, wave phase) With continuing wave action and after the maximum solute flux, oxygen-rich water is being filtered through the sediment, and mobile horizontal oxygen concentration gradients may develop (Shum 1993). Ensuing alternating exposure to variable redox conditions may result in more complete and rapid decomposition of organic material trapped in the upper sediment layer (Aller 1994). An equilibrium solute flux develops, and constant intrusion of oxygen-rich water into the sediment may increase overall oxygen penetration depth into the sediment. (e, calm phase) After the wave event, the water exchange across the interface is reduced to its original low value, filtering is reduced, solute concentrations increase in the sediment, and the former oxygen penetration depth is reinstated.

depth of 234 m at least once over a 3-yr period. Wiberg and Harris (1994) showed the effects of water depth, wave height, wave period, and sediment grain size on ripple formation. They calculated that orbital ripples could form at a water depth of 100 m with a wave period of 12 s, 4 m wave height, and a sediment grain size of 250 $\mu$m.

On the basis of literature cited throughout the present article and our results, we suggest that the coastal and shelf seas can be divided into four depth zones that show different sediment-water interaction processes due to surface gravity waves (Fig. 7). The first and uppermost zone (not addressed in the present study) is the beach, where the run-up of waves may cause filtering rates of up to 85 $m^3$ $m^{-1}$ $d^{-1}$ (McLachlan 1989), which equals, dependent on the lateral extension of the filtering zone, $\sim$1,000 L $m^{-2}$ $d^{-1}$. The second zone is made up of those shallow areas where the sediment is nearly permanently exposed to oscillating currents that cause filtration when they interact with bed topography. In the third zone, wave orbital motion reaches the seafloor only episodically, and in the fourth zone it never does. In the latter zone, wave-induced hydrostatic pressure oscillations may enhance sediment-water fluid exchange. The lateral extension of these zones varies, depending on the shelf slope and wave regime. With filtering rates of $\sim$1,000 L $m^{-2}$ $d^{-1}$ in beaches, 100 L $m^{-2}$ $d^{-1}$ caused by ripple-flow interaction, $\sim$30 L $m^{-2}$ $d^{-1}$

by wave pumping (Riedl et al. 1972; Mu et al. 1999), and molecular diffusion equivalent to a fluid exchange rate of $\sim$10 L $m^{-2}$ $d^{-1}$, the ratio among the average rates caused by the four transport processes may be roughly $100:10:3:1$.

The wave-induced filtering, thus, generally increases with decreasing water depth, and our study suggests that this increase is not steady but displays stepwise changes in its increase rates because of the dominance of different wave-driven exchange processes in the four depth zones (Fig. 7). This is most obvious at the interface of the sublittoral zone and the adjacent beach. However, the boundary between zones with and without wave ripples can be abrupt and sharp, and we can expect a jump in the filtration rate between those areas, as indicated by the sudden increase of flushing rate with evolving topography in our flume experiments. The changing magnitude of the filtration rate with depth may have ecological consequences that are linked to the associated changes in transport rates of metabolites into and out of the sediment.

In the second zone, where waves have the strongest impact on the submerged seafloor, ripples are permanent features of the sediment surface, and steady advection leads to a complete and permanent flushing of the upper sediment layers, which therefore may be relatively rich in oxygen. Permanent advective transport of fine particles into the sed-

iment and steady flushing of decomposition products from the bed may convert these areas into efficient biocatalytic filters (Huettel et al. 1998).

In our experiments, we measured strong initial pulses of solute release from the sandy sediment when ripples were formed. Such a scenario may take place in the third zone, where surface gravity waves reach the seafloor only episodically. The nutrient pulses Oldham and Lavery (1999) measured in such an environment could be attributed to this effect. Figure 8 proposes a sequence describing the solute fluxes across the sediment-water interface during an episodical storm event in the shallow, sandy shelf environment.

*Applicability of experiments*—Our experimental sediment had a grain size distribution of 100–300 $\mu$m, which may be representative for the most common grain size on the continental shelves. Cacchione et al. (1999) and Ogston and Sternberg (1999), for example, described shelf sands with a grain size distribution of 125 and 250 $\mu$m and ripples with 9 cm wavelength at 60 m water depth. Additionally, large areas of the shelves are covered by coarser, more permeable sediments (e.g., Emery 1968; Marinelli et al. 1998; Black and Oldman 1999), where advective processes may be much stronger than those observed in our flume experiments. The advective flux we observed during our experiments was mainly caused by the interaction of sediment topography and boundary layer flow. All topography evolved as the response of the bed to the hydrodynamic conditions during the respective experiments. No artificial roughness elements were placed or built on the sediment surface. Thus, the bed roughness was in equilibrium with the surface gravity waves, and the observed solute flux was not exaggerated by, for example, oversized sediment topography.

However, under laboratory conditions, wave ripples may form that are different to those common in nature. Wiberg and Harris (1994) showed that most laboratory experiments produce orbital ripples, with ripple spacing proportional to the wave orbital diameter, and this was also the case in our experiments. In nature, nearly all wave ripples are of the anorbital or suborbital type, and their wavelengths are proportional to sediment grain size rather than to wave properties. For a natural environment, Wiberg and Harris (1994) predicted a ripple spacing of $\sim$10 cm for sand with a median grain size of 200 $\mu$m, which results in about one third of the ripples per unit area as in our experiments. Even with only one third of ripples per unit surface area and on the basis of the maximum but conservative filtering rate of 590 L m$^{-2}$ d$^{-1}$ we recorded, this would result in a filtering rate of $\sim$200 L m$^{-2}$ d$^{-1}$.

We suggest that the numerical approaches developed to calculate advective filtering under unidirectional flow can be used to obtain conservative estimates of wave-induced advective exchange. We can estimate the magnitude and importance of these processes by applying these relationships to field data from previous studies. Cacchione et al. (1999) presented data from the Eel continental shelf, situated at $\sim$50 m water depth. Using values of 40 cm s$^{-1}$ for $u$ (120 cm over sediment), 9 cm ripple amplitude, 1.1 cm ripple height (calculated with a ripple steepness of 0.12; Wiberg and Harris 1994), and 1.5 $\times$ 10$^{-11}$ m$^2$ permeability (assumed to be

similar to that in the present study because of the similar grain size), we obtained a filtering rate of 103 L m$^{-2}$ d$^{-1}$. Li and Amos (1999) conducted a field study on the Nova Scotia shelf at 56 m water depth. With a maximal wave-induced $u$ = 25 cm s$^{-1}$ (50 cm over sediment), ripple amplitude $L_D$ = 9 cm; (calculated) ripple height $\delta$ = 1.1 cm, and an assumed permeability of 1.5 $\times$ 10$^{-11}$ m$^2$, we calculated 68 L m$^{-2}$ d$^{-1}$ of advective filtering during single events, whereas, during calmer periods with bottom currents below 10 cm s$^{-1}$, calculated filtering was reduced to 11 L m$^{-2}$ d$^{-1}$. On the basis of these calculations and our experimental findings, we conclude that 50–100 L m$^{-2}$ d$^{-1}$ is a moderate value for advective filtering in permeable shelf sediments exposed to oscillating flow. Sediments only episodically reached by waves may display similar filtering rates but only during storm events. In these beds, however, wave pumping by hydrostatic pressure oscillations may constantly enhance solute release.

The ecological relevance of wave-induced filtration is linked to the high load of organic matter commonly present in nearshore waters. In contrast to continuous pore-water advection caused by constant unidirectional flow, wave-induced pore-water exchange is characterized by pulsing flow due to the constant acceleration and deceleration of the boundary current. These pulsing flows can transport particulate matter efficiently through the pore space, thereby enhancing the filtration capacity of the bed. Surface gravity waves convert the sand sediments ubiquitous in the shallow shelf into effective filter systems, which suggests that these beds are sites for rapid mineralization and recycling.

## References

ALLER, R. C. 1982. The effects of macrobenthos on chemical properties of marine sediment and overlying water, p. 53–102. *In* P. L. McCall and M. J. S. Tevesz [eds.], Animal-sediment relations. Plenum.

———. 1994. Bioturbation and remineralization of sedimentary organic matter: effects of redox oscillation. Chem. Geol. **114:** 331–345.

———. 2001. Transport and reactions in the bioirrgated zone, p. 269–301. *In* B. P. Boudreau and B. B. Jørgensen [eds.], The benthic boundary layer. Oxford Univ. Press.

BERNER, R. A. 1980. Early diagenesis—a theoretical approach. Princeton Univ. Press.

BLACK, K. P., AND J. W. OLDMAN. 1999. Wave mechanisms responsible for grain sorting and non-uniform ripple distribution across two moderate-energy, sandy continental shelves. Mar. Geol. **162:** 121–132.

CACCHIONE, D. A., P. L. WIBERG, J. LYNCH, J. IRISH, AND P. TRAYKOVSKI. 1999. Estimates of suspended-sediment flux and bedform activity on the inner portion of the Eel continental shelf. Mar. Geol. **154:** 83–97.

CALDWELL, D. R., AND T. M. CHRISS. 1979. The viscous sublayer at the sea floor. Science **205:** 1131–1132.

DENNY, M. W. 1988. Biology and the mechanics of the wave-swept environment. Princeton Univ. Press.

ELLIOTT, A. H. 1990. Transfer of solutes into and out of streambeds. Ph.D. thesis, California Institute of Technology.

EMERY, K. O. 1968. Relict sediments on continental shelves of the world. Am. Assoc. Pet. Geol. Bull. **52:** 445–464.

FORSTER, S., M. HUETTEL, AND W. ZIEBIS. 1996. Impact of boundary layer flow velocity on oxygen utilisation in coastal sediments. Mar. Ecol. Prog. Ser. **143:** 173–185.

HARRIS, C. K., AND P. L. WIBERG. 1997. Approaches to quantifying long-term continental shelf sediment transport with an example from the Northern California STRESS mid-shelf site. Cont. Shelf Res. **17:** 1389–1418.

HARRIS, P. T., AND R. COLEMAN. 1998. Estimating global shelf sediment mobility due to swell waves. Mar. Geol. **150:** 171–177.

HARRISON, W. D., D. MUSGRAVE, AND W. S. REEBURGH. 1983. A wave-induced transport process in marine sediments. J. Geophys. Res. **88:** 7617–7622.

HSÜ, K. J. 1989. Physical principles of sedimentology. Springer Verlag.

HUETTEL, M., AND G. GUST. 1992. Impact of bioroughness on interfacial solute exchange in permeable sediments. Mar. Ecol. Prog. Ser. **89:** 253–267.

———, AND A. RUSCH. 2000. Transport and degradation of phytoplankton in permeable sediment. Limnol. Oceanogr. **45:** 534–549.

———, AND I. T. WEBSTER. 2001. Porewater flow in permeable sediments, p. 144–179. *In* B. P. Boudreau and B. B. Jørgensen [eds.], The benthic boundary layer. Oxford Univ. Press.

———, W. ZIEBIS, AND S. FORSTER. 1996. Flow-induced uptake of particulate matter in permeable sediments. Limnol. Oceanogr. **41:** 309–322.

———, ———, ———, AND G. I. LUTHER. 1998. Advective transport affecting metal and nutrient distribution and interfacial fluxes in permeable sediments. Geochim. Cosmochim. Acta **62:** 613–631.

KLUTE, A., AND C. DIRKSEN. 1986. Hydraulic conductivity and diffusivity: Laboratory methods, p. 687–734. *In* A. Klute [ed.], Methods of soil analysis. Part 1, Physical and mineralogical methods. American Society of Agronomy.

KRÖGEL, F. 1997. Einfluß von Viskosität und Dichte des Seewassers auf Transport und Ablagerung von Wattsedimenten (Langeooger Rückseitenwatt, südliche Nordsee). Berichte aus dem Fachbereich Geowissenschaften der Universität Bremen. 102.

LI, M. Z., AND C. L. AMOS. 1999. Field observations of bedforms and sediment transport thresholds of fine sand under combined waves and currents. Mar. Geol. **158:** 147–160.

MALAN, D. E., AND A. MCLACHLAN. 1991. In situ benthic oxygen fluxes in a nearshore coastal marine system: A new approach to quantify the effect of wave action. Mar. Ecol. Prog. Ser. **73:** 69–81.

MARINELLI, R. L., R. A. JAHNKE, D. B. CRAVEN, J. R. NELSON, AND J. E. ECKMAN. 1998. Sediment nutrient dynamics on the South Atlantic Bight continental shelf. Limnol. Oceanogr. **43:** 1305–1320.

MCLACHLAN, A. 1989. Water filtration by dissipative beaches. Limnol. Oceanogr. **34:** 774–780.

MU, Y. K., A. H. D. CHENG, M. BADIEY, AND R. BENNETT. 1999. Water wave driven seepage in sediment and parameter inversion based on pore pressure data. Int. J. Num. Anal. Methods Geomech. **23:** 1655–1674.

OGSTON, A. S., AND R. W. STERNBERG. 1999. Sediment-transport events on the northern California continental shelf. Mar. Geol. **154:** 69–82.

OLDHAM, C. E., AND P. S. LAVERY. 1999. Porewater nutrient fluxes in a shallow fetch-limited estuary. Mar. Ecol. Prog. Ser. **183:** 39–47.

REY, V., A. G. DAVIES, AND M. BELZONS. 1995. On the formation of bars by the action of waves on an erodible bed—a laboratory study. J. Coast. Res. **11:** 1180–1194.

RIEDL, R. J., N. HUANG, AND R. MACHAN. 1972. The subtidal pump: A mechanism of interstitial water exchange by wave action. Mar. Biol. **13:** 210–221.

RUTGERS VAN DER LOEFF, M. M. 1981. Wave effects on sediment water exchange in a submerged sand bed. Neth. J. Sea Res. **15:** 100–112.

RUTHERFORD, J. C., J. D. BOYLE, A. H. ELLIOTT, T. V. J. HATHERELL, AND T. W. CHIU. 1995. Modeling benthic oxygen-uptake by pumping. J. Environ. Eng. ASCE **121:** 84–95.

SAVANT, S. A., D. D. REIBLE, AND L. J. THIBODEAUX. 1987. Convective transport within stable river sediments. Water Resour. Res. **23:** 1763–1768.

SHUM, K. T. 1992. Wave-induced advective transport below a rippled water-sediment interface. J. Geophys. Res. **97:** 789–808.

———. 1993. The effects of wave-induced pore water circulation on the transport of reactive solutes below a rippled sediment bed. J. Geophys. Res. **98:** 10289–10301.

———, AND B. SUNDBY. 1996. Organic matter processing in continental shelf sediments—the subtidal pump revisited. Mar. Chem. **53:** 81–87.

THIBODEAUX, L. J., AND J. D. BOYLE. 1987. Bedform-generated convective transport in bottom sediment. Nature **325:** 341–343.

WEBB, J. E., AND J. L. THEODOR. 1968. Irrigation of submerged marine sands through wave action. Nature **220:** 682–683.

———, AND ———. 1972. Wave-induced circulation in submerged sands. J. Mar. Biol. Assoc. U.K. **52:** 903–914.

WEBSTER, I. T., S. J. NORQUAY, F. C. ROSS, AND R. A. WOODING. 1996. Solute exchange by convection within estuarine sediments. Estuar. Coast. Shelf Sci. **42:** 171–183.

WIBERG, P. L., AND C. K. HARRIS. 1994. Ripple geometry in wave-dominated environments. J. Geophys. Res. **99:** 775–789.

ZIEBIS, W., M. HUETTEL, AND S. FORSTER. 1996. Impact of biogenic sediment topography on oxygen fluxes in permeable seabeds. Mar. Ecol. Prog. Ser. **140:** 227–237.